Biochemical and Biophysical Research Communications 453 (2014) 25–30

Contents lists available at ScienceDirect

Biochemical and Biophysical Research Communications

journal homepage: www.elsevier.com/locate/ybbrc

Crystal structure of the human CSN6 MPN domain

Xiao-li Ma [a,b], Min Xu [a,*], Tao Jiang [a,*]

[a] National Laboratory of Biomacromolecules, Institute of Biophysics, Chinese Academy of Sciences, Beijing 100101, China
[b] University of Chinese Academy of Sciences, 19A Yuquan Road, Shijingshan District, Beijing 100039, China

ARTICLE INFO

Article history:
Received 26 August 2014
Available online 19 September 2014

Keywords:
COP9 signalosome
CSN6
MPN domain
JAMM motif
Isopeptidase activity
Deneddylation

ABSTRACT

The mammalian COP9 signalosome is an eight-subunit (CSN1–CSN8) complex that plays essential roles in multiple cellular and physiological processes. CSN5 and CSN6 are the only two MPN (Mpr1-Pad1-N-terminal) domain-containing subunits in the complex. Unlike the CSN5 MPN domain, CSN6 lacks a metal-binding site and isopeptidase activity. Here, we report the crystal structure of the human CSN6 MPN domain. Each CSN6 monomer contains nine β sheets surrounded by three helices. Two forms of dimers are observed in the crystal structure. Interestingly, a domain swapping of β8 and β9 strands occurs between two neighboring monomers to complete a typical MPN fold. Analyses of the pseudo metal-binding motif in CSN6 suggest that the loss of two key histidine residues may contribute to the lack of catalytic activity in CSN6. Comparing the MPN domain of our CSN6 with that in the CSN complex shows that apart from the different β8–β9 conformation, they have minor conformational differences at two insertion regions (Ins-1 and Ins-2). Besides, the interacting mode of CSN6–CSN6 in our structure is distinct from that of CSN5–CSN6 in the CSN complex structure. Moreover, the functional implications for Ins-1 and Ins-2 are discussed.

1. Introduction

The constitutive photomorphogenesis 9 (COP9) signalosome (CSN) was initially identified as a repressor of constitutive photomorphogenesis in *Arabidopsis* [1,2], and subsequently found in a variety of eukaryotic organisms including *Saccharomyces cerevisiae* [3,4], *Schizosaccharomyces pombe* [5], *Caenorhabditis elegans* [6], *Drosophila melanogaster* [7] and mammals [8,9]. The predominant biochemical function of the CSN complex is its isopeptidase catalytic activity, which deneddylates the ubiquitin-like protein NEDD8 of the Cullin–RING family of ubiquitin E3 ligases (CRLs) and thereby regulates the activity of CRLs. The CSN complex plays a key role in protein degradation and is involved in a variety of cellular and physiological processes including cell cycle checkpoint controls, embryonic development, signal transduction, and transcriptional regulation (see review Wei & Deng [10]).

This highly evolutionarily conserved protein complex typically consists of 8 subunits, CSN1 to CSN8, named in order of decreasing size. Among these components, six subunits (CSN1-4, 7, 8) contain a PCI domain (the 26S proteasome lid subcomplex, COP9 signalosome and initiation factor), while CSN5 and CSN6 share a conserved MPN domain (Mpr1-Pad1-N-terminal). Two types of MPN domains have been found in many studies: the JAMM/MPN$^+$ domain contains a metal-binding JAMM (Jab1/MPN/Mov34) motif that typically consists of a conserved EX_nHS/THX_7SX_2D sequence that is responsible for its isopeptidase catalytic activity [11–14]. The other MPN$^-$ domain has no such motif, thus lacks isopeptidase activity [15–17]. The CSN-mediated deneddylation process depends on CSN5, which contains the JAMM motif characterized by a zinc-binding site and forms an isopeptidase catalytic pocket for deneddylation. However, CSN5 has no isopeptidase activity unless it is associated with other subunits [12,18]. Although the MPN$^-$ domain of CSN6 has no isopeptidase catalytic activity, previous electron microscopy studies have revealed that CSN5 extends from the plane of the PCI subunit cluster, and the MPN domains of CSN5 and CSN6 are connected [19]. This suggests that the MPN$^-$ domain of CSN6 may serve as a scaffold for CSN complex assembly, in particular by bridging peripheral CSN5 to the other subunits. In addition to the scaffold function, CSN6 has been shown to promotes tumorigenesis in mammalian cells by impacting ubiquitin-mediated proteolysis of important mediator in carcinogenesis and cancer progression [20,21].

The crystal structures of the MPN-containing human CSN5 subunit (1–257aa) [22] and a partial CSN6 MPN$^-$ domain from *D. melanogaster* [17] have been determined. In the latter structure, approximately 20 residues at the C-terminal were truncated, and the topology of the remaining C-terminal portion (residues

* Corresponding authors. Fax: +86 10 64888510 (T. Jiang).
E-mail addresses: xumin@moon.ibp.ac.cn (M. Xu), tjiang@ibp.ac.cn (T. Jiang).

http://dx.doi.org/10.1016/j.bbrc.2014.09.046
0006-291X/

143–184) is atypical [23]. To gain structural insight into the full length CSN6 MPN domain in humans, we solved the crystal structure of the human CSN6 MPN$^-$ domain (39–191aa) at 2.6 Å resolution. Interestingly, a domain swapping of β8 and β9 strands occurs between two neighboring monomers to form a typical MPN fold.

2. Materials and methods

2.1. Protein expression and purification

A gene fragment encoding the CSN6 MPN domain (residues 38–210) was cloned into pET24a between the *Nde*I and *Xho*I sites with a C-terminal 6-His tag. The plasmid was transformed into Rosetta (DE3) cells for expression. The expressed protein was purified to homogeneity by Ni affinity chromatography followed by Resource Q chromatography and Superdex™200 HR 10/300 gel filtration. The dimer fractions were collected and concentrated to ~8 mg/ml in 20 mM Tris–HCl pH 8.0, 100 mM NaCl for crystallization.

Mutant CSN6 was designed using an existing CSN6$_{38–210}$ clone in pET24a. Five single mutants (D53G, R57G, Q61G, E88G and Y104G), three double mutants (Q61G/E88G, R57G/Y104G and Q61G/Y104G) and one triple mutant (Q61G/Y104G/E88G) were constructed. The cell culture and protein purification procedures were the same as that of wide type CSN6.

2.2. Crystallization and data collection

Crystals were grown at 16 °C by the hanging drop method using equal volumes of protein and crystallization solution over a 1 mL reservoir. The reservoir contained 0.1 M Tris pH 7.7 and 26% (w/v) PEG4000. Mercurated crystals were obtained by adding ethyl mercuric phosphate to the hanging drop, to a final concentration of 2.5 mM, and soaking the crystals for approximately 5 h. The diffraction of the crystals improved to 2.6 Å after dehydration in 15% (w/v) xylosic alcohol, 0.1 M Tris pH 7.7, 26% (w/v) PEG4000 [24]. The crystals were flash-frozen in liquid nitrogen before data collection. Diffraction data were collected on beamline BL-17A at the Photon Factory in Japan and processed with HKL2000 [25].

2.3. Structure determination and refinement

The crystal belonged to space group $P3_2$ with a dimer in the asymmetric unit. The phase was determined by the single wavelength anomalous dispersion method (SAD), using the mercury-derivatized protein crystals. Electron density maps were calculated by PHENIX [26,27]. Model building was done using COOT [28], and refined with PHENIX [26,29]. The final R_{work} and R_{free} values were 22.1% and 25.6%, respectively. The final structure was analyzed with PROCHECK [30]. Data collection and refinement statistics are presented in Table 1. Structure figures were prepared using PyMol (http://www.pymol.org), and the coordinates were deposited in the PDB under accession code 4R14.

2.4. Analytical ultracentrifugation

Sedimentation velocity measurements were performed on a Beckman's ProteomeLab XL-I at 25 °C. All protein samples were diluted to an OD 280 nm of 0.7 in 20 mM HEPES, pH 7.5, 150 mM NaCl. Data were collected at 60,000 r.p.m. (262,000 g) every 3 min at a wavelength of 280 nm. Interference sedimentation coefficient distributions, c(M), were calculated from the sedimentation velocity data by using SEDFIT [31].

Table 1
Data collection and refinement statistics.

	CSN6 (Hg-derivative)
Data collection	
Space group	$P3_2$
Wavelength (Å)	1.0055
Resolution (Å)	50–2.6 (2.64–2.6)
Cell dimensions	
a, *b*, *c* (Å)	66.55, 66.55, 86.83
α, β, γ (°)	90, 90, 120
Unique reflections	13,213 (650)
I/σ (I)	56.35 (7.00)
Completeness (%)	99.8 (100)
R_{merge} (%)[a]	6.1 (53.9)
Wilson B factor (Å)	31.79
Refinement	
R_{work} (%)[b]	22.1
R_{free} (%)[c]	25.6
Average B factors (Å)	
Protein	53.79
Hg	47.84
Total	53.77
Root mean square deviations	
Bond length (Å)	0.010
Bond angles (°)	1.135
Ramachandran plot	
Most favored (%)	93.42
Additionally allowed (%)	6.58
Generously allowed (%)	0
Disallowed	0

Numbers in parentheses represent statistics for the highest resolution shell.
[a] $R_{merge} = \sum|I - \langle I\rangle|/\sum I$, where I is the measured intensity for reflections with indices *hkl*.
[b] $R_{work} = \sum||F_{obs}| - |F_{calc}||/\sum|F_{obs}|$.
[c] R_{free} = R factor for a selected subset (5%) of the reflections that were not included in prior refinement calculations.

3. Results and discussion

3.1. Overall structure of CSN6$_{39–191}$

We have purified and crystallized a soluble form of the human CSN6 MPN$^-$ domain containing residues 38–210. The crystal structure was solved by single wavelength anomalous dispersion (SAD) using crystals derivatized with ethyl mercuric phosphate. The crystal belongs to the space group $P3_2$ and contains a dimer in the asymmetric unit. The structure of CSN6 contains residues 39–191; residues 192–210 were not observed in the crystal.

Structural analysis reveals that, unlike the atypical C-terminal MPN fold (residues 143–184) of *D. melanogaster* CSN6$_{51–184}$, human CSN6$_{39–191}$ adopts a typical MPN topology primarily composed of nine β-strands and three α-helices (Fig. 1), which is similar to a number of other MPN$^-$-containing proteins [13,15,16,22,32]. Interestingly, there is a domain swap between two neighboring CSN6 molecules. When compared to other MPN-containing protein structures observed to date [13,15,16,22,32], the human CSN6 structure is unique; the β8 and β9 strands of molecule A are stretched out, and their positions are occupied by the β8′ and β9′ strands from molecule B′ in the neighboring asymmetric unit, thereby completing a typical MPN fold (Fig. 1B). This swapped domain is connected to the rest of the protein by a large flexible hinge that connects β7 and β8.

3.2. The oligomeric state of CSN6$_{39–191}$

To obtain a homogeneous protein sample suitable for crystallization, the CSN6 protein was purified by size exclusion chromatography using a Superdex 200 column. We observed CSN6 in both monomeric and dimeric states in solution (Fig. 2B), indicating that

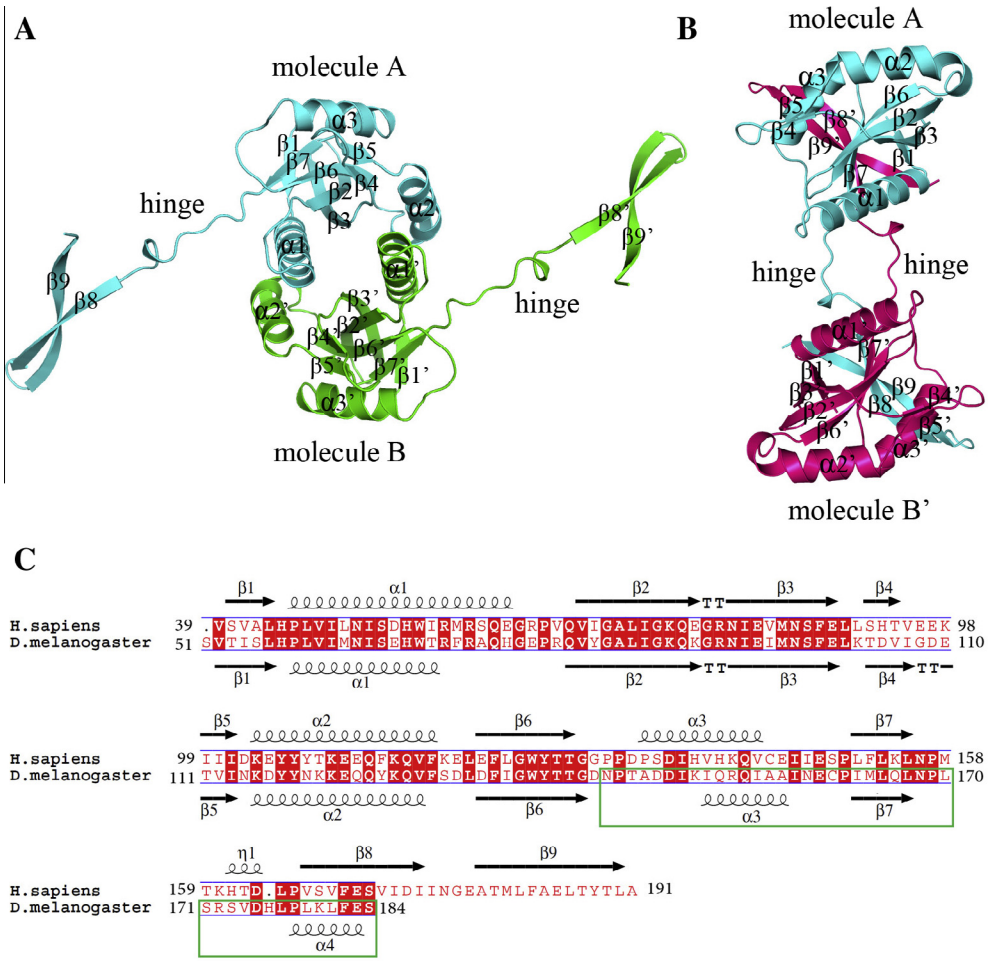

Fig. 1. Overall structure of $CSN6_{39-191}$ and structure based sequence alignment of *H. sapiens* and *D. melanogaster* CSN6. (A) The AB dimer. (B) The AB′ dimer. Molecule A is colored in cyan, molecule B is colored in green, and molecule B′ is colored in hot pink. (C) Structure-based sequence alignment of H. sapiens and *D. melanogaster* CSN6. The differences in structural fold topology are indicated by a green box. (For interpretation of the references to color in this figure legend, the reader is referred to the web version of this article.)

there may be equilibrium between the two oligomeric forms. The dimeric protein peak was collected for crystallization, and accordingly two stable dimeric forms were observed in the crystal structure. The first is formed by two molecules in an asymmetric unit, referred to as a type AB dimer (Fig. 1A); the second is formed by domain swapping between two molecules in the neighboring asymmetric units, referred to as a type AB′ dimer (Fig. 1B). The AB dimer is mainly formed by hydrophilic interactions between key residues in the α1 and α2 helices and the β3 strand on both subunits. In the interface, hydrogen bonds are formed between the side chains of D53, R57, Q61, E88 and Y104 of both subunits, which make the two molecules bind tightly (Fig. 2A). The AB′ dimer arises mainly through interactions between the β7–β8′ antiparallel strands and the β1–β9′ parallel strands. The total buried surface areas in the AB and AB′ dimers are 722.8 Å^2 and 2023.1 Å^2, respectively.

To elucidate which dimer form exists in solution, structurally guided mutations were introduced. Residues D53, R57, Q61, E88 and Y104, contribute significantly to AB dimerization and were selected for glycine substitution. These single mutants showed little change in their elution volumes by size exclusion (data not shown), suggesting that these single mutations have little effect in disrupting the dimerization, likely because of the robust hydrogen bond network in the dimer interface. Hence, four double or triple mutants, Q61G/Y104G, R57G/Y104G, Q61G/E88G and Q61G/E88G/Y104G were further selected and tested. Compared with wild type CSN6, these four mutants all behave as monomers and show a significant shift in size-exclusion chromatography (Fig. 2B). We took the Q61G/Y104G mutant protein to perform analytical ultracentrifugation experiments to corroborate the oligomeric state of this mutant. Like the size-exclusion results, the Q61G/Y104G mutant has a calculated molecular mass of 21.143 kD, indicating a monomeric state (Fig. 2C). This result indicates that dimerization is significantly disrupted via these four mutants, indicating that the AB dimer is the dimeric form of CSN6 existing in solution.

Dimerization has also been found in other MPN^- containing proteins including Mov34 and CSN5. However, it is noteworthy that these dimer assemblies form via totally different interfaces. The Mov34 dimer is formed by numerous interactions between the α1, α2 and α4 helices and the CSN5 dimer is formed by interactions between the Ins-1 segment and the α4 helix. The functional relevance of these different dimer forms is not clear and further investigations are needed.

3.3. The pseudo metal-binding site in CSN6

Human CSN6 lacks a real JAMM motif and no metal or water is found in the corresponding region of the structure (Fig. 3A). When comparing the zinc-binding site of CSN5 with the equivalent region in CSN6, several residues that are similar to the JAMM motif

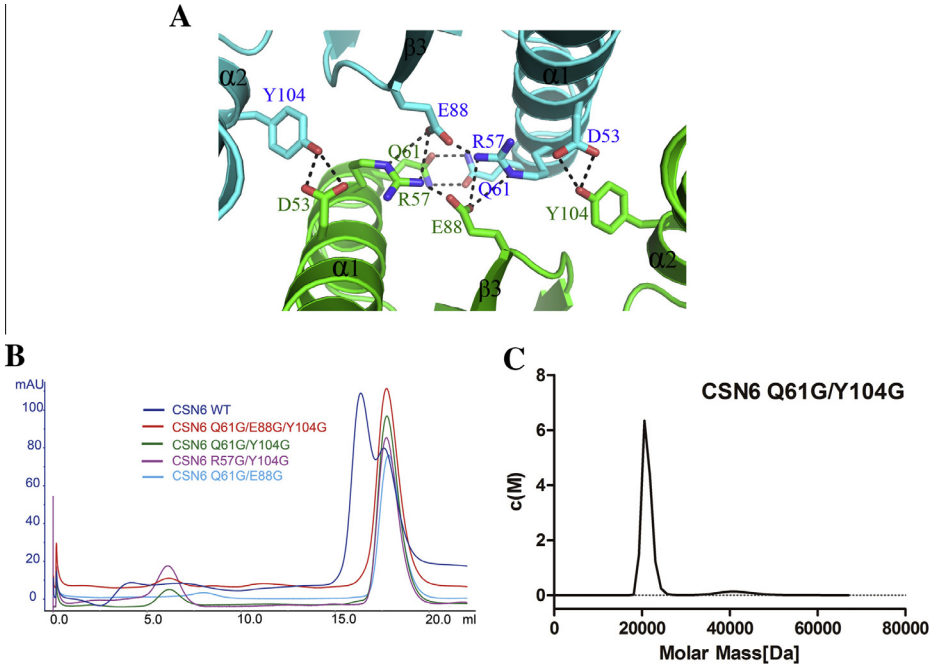

Fig. 2. The interface between molecule A and molecule B. (A) The key residues contributing to the dimerization are labeled and shown in stick. (B) Size exclusion profiles of wide type CSN6 MPN domain and four mutants. Protein samples were loaded on a Superdex 200 HR 10/300 column for gel filtration assays. (C) Analytical ultracentrifugation analysis of the Q61G/Y104G mutant.

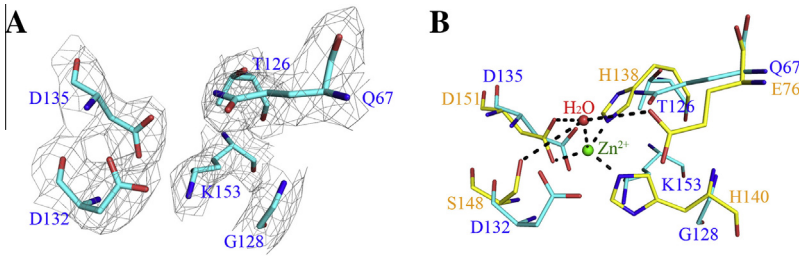

Fig. 3. The pseudo metal-binding site in CSN6. (A) The electron density for the residues corresponding to the zinc-binding site of CSN6. $2|F_o|-|F_c|$ map is contoured at 1.0σ, showing that there is no metal or water in the region. (B) Superposition of the zinc-binding site of CSN5 with the equivalent region on CSN6.

are found and appear to form a pseudo metal-binding site. As shown in Fig. 3B, the residues Q67, D132 and D135 in CSN6 are structurally equivalent to E76, S148 and D151 in CSN5, respectively. However, the replacement of H138 and H140 residues in CSN5 by T126 and G128 in CSN6 disrupts the zinc coordination site, thus abolishes the metal-binding ability of CSN6. Although the K153 in CSN6 occupies the side chain position of H140 in CSN5 and restores some negative charge of histidine, it is not sufficient to re-establish an active isopeptidase pocket.

3.4. The Ins-1 region of CSN6

Previous studies indicated that two insertions, Ins-1 and Ins-2, are observed among various MPN domains. These segments were originally described in the AMSH-LP structure [32].

The Ins-1 segment in CSN5 is mainly helical. In Mov34, AMSH-LP/AMSH and our CSN6 structure, it contains a β-hairpin followed by a long helix (Fig. 4). The Ins-1 segment appears to affect the activation of the JAMM/MPN$^+$ proteins. In the structure of CSN5, the Ins-1 segment blocks the isopeptidase pocket by inserting R106 into the active site [22]; while in AMSH-LP, Ins-1 covers the zinc-binding active site with D321 and interacts with C-terminal tail of ubiquitin by its β-hairpin [32]. Comparing the Ins-1 β-hairpins of AMSH-LP, Mov34 and CSN6 reveals that the β-hairpin in the MPN$^+$ protein AMSH-LP is in very close proximity to the active site, whereas in the MPN$^-$ proteins CSN6 and Mov34, the β-hairpins are relatively far from the pseudo active site (Fig. 4). Moreover, superposition of *D. melanogaster* $CSN6_{51-184}$ N-terminal MPN domain and our human CSN6 structure also reveals that the β-hairpins are oriented at slightly different angles (Fig. 4D). It is possible that the flexibility of the Ins-1 β-hairpin in CSN6 contributes to the accommodation of substrate.

3.5. The Ins-2 region and the hinge connecting β7 and β8

Like the Ins-1 segment, Ins-2 varies greatly among MPN-containing proteins. In CSN5, it is disordered and invisible. In AMSH-LP, it contains a long helix and a following flexible loop and in Mov34 and human CSN6, it forms a β-hairpin (Fig. 4). Studies have demonstrated that the Ins-2 region of AMSH-LP covers the zinc-binding active site with a protruding F407, which interacts with its di-ubiquitin substrate [32]. However, the role of the Ins-2 segment in other MPN-containing proteins is not clear.

When we were preparing this manuscript, a holo-CSN complex (CSN1–8) structure was reported [33]. In the holo-CSN complex, the single copy of CSN6 forms a heterodimer with CSN5 without

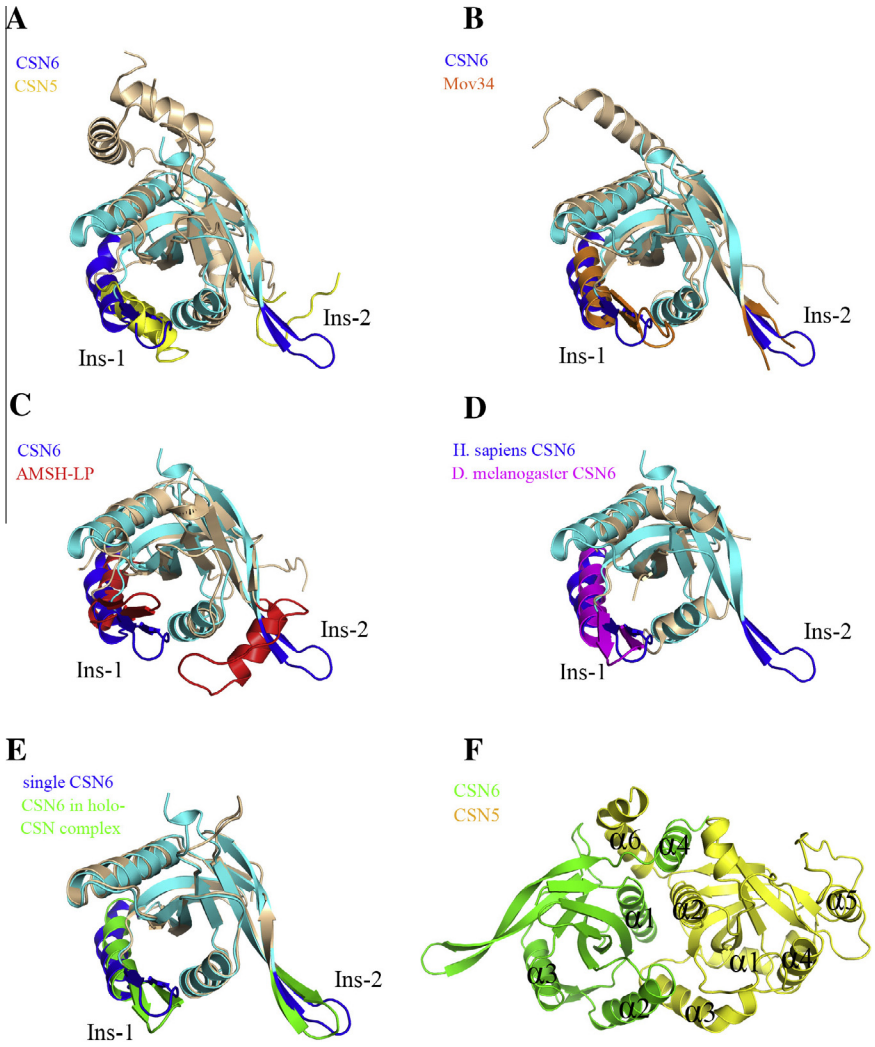

Fig. 4. Structural superposition of human $CSN6_{39-191}$ with MPN-containing proteins: CSN5, Mov34, AMSH-LP, Drosophila CSN6 and CSN6 in holo-CSN complex. The monomer $CSN6_{39-191}$ used is completed by the β8′ and β9′ strands of molecule B′ and the rest of the structure of molecule A. (A–E) Human $CSN6_{39-191}$ is shown in cyan except that the Ins-1 and Ins-2 segments are in blue. Other proteins are in wheat except that the Ins-1 and Ins-2 segments of CSN5 are in yellow, Mov34 is in orange, AMSH-LP is in red, Drosophila CSN6 is in magenta and CSN6 in holo-CSN complex is in green. (F) Heterodimer of CSN5 and CSN6 in holo-CSN complex. CSN5 is in yellow and CSN6 is in green. In the holo-CSN complex, the single copy of CSN6 forms a heterodimer with CSN5. (For interpretation of the references to color in this figure legend, the reader is referred to the web version of this article.)

domain swapping of the β8–β9 strands. Comparison of the CSN6 MPN domain in the two structures shows that apart from possessing different β8–β9 conformation which is involved in domain swapping in our CSN6 structure, the two structures have minor conformational differences at Ins-1 and Ins-2 regions, as shown in Fig. 4E.

Moreover, we compared the dimer interface of the CSN6 MPN domain in our structure with the interacting interface between CSN5 and CSN6 MPN domains in the holo-CSN complex. In our CSN6 homodimer structure, α1 and α2 from one monomer interact with α2 and α1 from another monomer, respectively (Fig. 1A), while in the CSN5–CSN6 heterodimer, α1 and α2 helices of CSN6 pack to α2 and α3 of CSN5, respectively. Moreover, in the CSN5–CSN6 heterodimer, α4 helix of CSN6, a C-terminal extension of the MPN domain, interacts with α6 helix of CSN5 (Fig. 4F). Notably, α2, α3 and α6 helices of CSN5 are equivalent to α1, α2 and α4 helices of CSN6, respectively.

Furthermore, the holo-CSN complex structure shows that the Ins-2 β-hairpin in CSN6 interacts with CSN4 and the Ins-2 β-hairpin deletion yields more active complex than wild type, suggesting that the Ins-2 β-hairpin of CSN6 plays an important role in CSN activation. This, together with our observation of the stretching out of the Ins-2 β-hairpin-containing β8–β9 strands, indicates a need to further investigate the relationship between the movement of the flexible hinge connecting β7 and β8 and the association of CSN6 with other proteins.

Acknowledgments

We thank the staff at the BL17U beamline of the SSRF (Shanghai Synchrotron Radiation Facility) in China and the BL-17A beamline of the Photon Factory in Japan for technical assistance during data collection. This work was supported by grants from the National Basic Research Program of China (2011CB910302); the Strategic Priority Research Program (XDB08010301); and the National Natural Science Foundation of China (31025009, 31200558).

References

[1] N. Wei, D.A. Chamovitz, X.W. Deng, Arabidopsis COP9 is a component of a novel signaling complex mediating light control of development, Cell 78 (1994) 117–124.
[2] N. Wei, X.W. Deng, COP9: a new genetic locus involved in light-regulated development and gene expression in arabidopsis, Plant Cell 4 (1992) 1507–1518.

[3] V. Maytal-Kivity, E. Pick, R. Piran, K. Hofmann, M.H. Glickman, The COP9 signalosome-like complex in *S. cerevisiae* and links to other PCI complexes, Int. J. Biochem. Cell Biol. 35 (2003) 706–715.
[4] S. Wee, B. Hetfeld, W. Dubiel, D.A. Wolf, Conservation of the COP9/signalosome in budding yeast, BMC Genet. 3 (2002) 15.
[5] K.E. Mundt, J. Porte, J.M. Murray, C. Brikos, P.U. Christensen, T. Caspari, I.M. Hagan, J.B. Millar, V. Simanis, K. Hofmann, A.M. Carr, The COP9/signalosome complex is conserved in fission yeast and has a role in S phase, Curr. Biol. 9 (1999) 1427–1430.
[6] L. Pintard, T. Kurz, S. Glaser, J.H. Willis, M. Peter, B. Bowerman, Neddylation and deneddylation of CUL-3 is required to target MEI-1/Katanin for degradation at the meiosis-to-mitosis transition in *C. elegans*, Curr. Biol. 13 (2003) 911–921.
[7] S. Freilich, E. Oron, Y. Kapp, Y. Nevo-Caspi, S. Orgad, D. Segal, D.A. Chamovitz, The COP9 signalosome is essential for development of *Drosophila melanogaster*, Curr. Biol. 9 (1999) 1187–1190.
[8] N. Wei, X.W. Deng, Characterization and purification of the mammalian COP9 complex, a conserved nuclear regulator initially identified as a repressor of photomorphogenesis in higher plants, Photochem. Photobiol. 68 (1998) 237–241.
[9] M. Seeger, R. Kraft, K. Ferrell, D. Bech-Otschir, R. Dumdey, R. Schade, C. Gordon, M. Naumann, W. Dubiel, A novel protein complex involved in signal transduction possessing similarities to 26S proteasome subunits, FASEB J. 12 (1998) 469–478.
[10] N. Wei, X.W. Deng, The COP9 signalosome, Annu. Rev. Cell Dev. Biol. 19 (2003) 261–286.
[11] R. Verma, L. Aravind, R. Oania, W.H. McDonald, J.R. Yates 3rd, E.V. Koonin, R.J. Deshaies, Role of Rpn11 metalloprotease in deubiquitination and degradation by the 26S proteasome, Science 298 (2002) 611–615.
[12] G.A. Cope, G.S. Suh, L. Aravind, S.E. Schwarz, S.L. Zipursky, E.V. Koonin, R.J. Deshaies, Role of predicted metalloprotease motif of Jab1/Csn5 in cleavage of Nedd8 from Cul1, Science 298 (2002) 608–611.
[13] H.J. Tran, M.D. Allen, J. Lowe, M. Bycroft, Structure of the Jab1/MPN domain and its implications for proteasome function, Biochemistry 42 (2003) 11460–11465.
[14] X.I. Ambroggio, D.C. Rees, R.J. Deshaies, JAMM: a metalloprotease-like zinc site in the proteasome and signalosome, PLoS Biol. 2 (2004) E2.
[15] M. Sanches, B.S. Alves, N.I. Zanchin, B.G. Guimaraes, The crystal structure of the human Mov34 MPN domain reveals a metal-free dimer, J. Mol. Biol. 370 (2007) 846–855.
[16] L. Zhang, J. Shen, M.T. Guarnieri, A. Heroux, K. Yang, R. Zhao, Crystal structure of the C-terminal domain of splicing factor Prp8 carrying retinitis pigmentosa mutants, Protein Sci. 16 (2007) 1024–1031.
[17] H. Zhang, Z.Q. Gao, W.J. Wang, G.F. Liu, E.V. Shtykova, J.H. Xu, L.F. Li, X.D. Su, Y.H. Dong, The crystal structure of the MPN domain from the COP9 signalosome subunit CSN6, FEBS Lett. 586 (2012) 1147–1153.
[18] M. Sharon, H. Mao, E. Boeri Erba, E. Stephens, N. Zheng, C.V. Robinson, Symmetrical modularity of the COP9 signalosome complex suggests its multifunctionality, Structure 17 (2009) 31–40.
[19] R.I. Enchev, D.C. Scott, P.C. da Fonseca, A. Schreiber, J.K. Monda, B.A. Schulman, M. Peter, E.P. Morris, Structural basis for a reciprocal regulation between SCF and CSN, Cell Rep. 2 (2012) 616–627.
[20] S.N. Zhang, D.S. Pei, J.N. Zheng, The COP9 signalosome subunit 6 (CSN6): a potential oncogene, Cell Div. 8 (2013) 14.
[21] R. Zhao, S.C. Yeung, J. Chen, T. Iwakuma, C.H. Su, B. Chen, C. Qu, F. Zhang, Y.T. Chen, Y.L. Lin, D.F. Lee, F. Jin, R. Zhu, T. Shaikenov, D. Sarbassov, A. Sahin, H. Wang, H. Wang, C.C. Lai, F.J. Tsai, G. Lozano, M.H. Lee, Subunit 6 of the COP9 signalosome promotes tumorigenesis in mice through stabilization of MDM2 and is upregulated in human cancers, J. Clin. Invest. 121 (2011) 851–865.
[22] A. Echalier, Y. Pan, M. Birol, N. Tavernier, L. Pintard, F. Hoh, C. Ebel, N. Galophe, F.X. Claret, C. Dumas, Insights into the regulation of the human COP9 signalosome catalytic subunit, CSN5/Jab1, Proc. Natl. Acad. Sci. U.S.A. 110 (2013) 1273–1278.
[23] M. Birol, A. Echalier, Structure and function of MPN (Mpr1/Pad1 N-terminal) domain-containing proteins, Curr. Protein Pept. Sci. (2014).
[24] B. Heras, J.L. Martin, Post-crystallization treatments for improving diffraction quality of protein crystals, Acta Crystallogr. D Biol. Crystallogr. 61 (2005) 1173–1180.
[25] Z. Otwinowski, W. Minor, Processing of X-ray diffraction data collected in oscillation mode, Methods Enzymol. 276 (1997) 307–326.
[26] P.D. Adams, P.V. Afonine, G. Bunkoczi, V.B. Chen, I.W. Davis, N. Echols, J.J. Headd, L.W. Hung, G.J. Kapral, R.W. Grosse-Kunstleve, A.J. McCoy, N.W. Moriarty, R. Oeffner, R.J. Read, D.C. Richardson, J.S. Richardson, T.C. Terwilliger, P.H. Zwart, PHENIX: a comprehensive Python-based system for macromolecular structure solution, Acta Crystallogr. Sect. D Biol. Crystallogr. 66 (2010) 213–221.
[27] T.C. Terwilliger, P.D. Adams, R.J. Read, A.J. McCoy, N.W. Moriarty, R.W. Grosse-Kunstleve, P.V. Afonine, P.H. Zwart, L.W. Hung, Decision-making in structure solution using Bayesian estimates of map quality: the PHENIX AutoSol wizard, Acta Crystallogr. Sect. D Biol. Crystallogr. 65 (2009) 582–601.
[28] P. Emsley, B. Lohkamp, W.G. Scott, K. Cowtan, Features and development of Coot, Acta Crystallogr. Sect. D Biol. Crystallogr. 66 (2010) 486–501.
[29] P.V. Afonine, R.W. Grosse-Kunstleve, N. Echols, J.J. Headd, N.W. Moriarty, M. Mustyakimov, T.C. Terwilliger, A. Urzhumtsev, P.H. Zwart, P.D. Adams, Towards automated crystallographic structure refinement with phenix.refine, Acta Crystallogr. D Biol. Crystallogr. 68 (2012) 352–367.
[30] R.A. Laskowski, M.W. MacArthur, D.S. Moss, J.M. Thornton, PROCHECK: a program to check the stereochemical quality of protein structures, J. Appl. Crystallogr. 26 (1993) 283–291.
[31] P. Schuck, Size-distribution analysis of macromolecules by sedimentation velocity ultracentrifugation and lamm equation modeling, Biophys. J. 78 (2000) 1606–1619.
[32] Y. Sato, A. Yoshikawa, A. Yamagata, H. Mimura, M. Yamashita, K. Ookata, O. Nureki, K. Iwai, M. Komada, S. Fukai, Structural basis for specific cleavage of Lys 63-linked polyubiquitin chains, Nature 455 (2008) 358–362.
[33] G.M. Lingaraju, R.D. Bunker, S. Cavadini, D. Hess, U. Hassiepen, M. Renatus, E.S. Fischer, N.H. Thoma, Crystal structure of the human COP9 signalosome, Nature (2014).